Motions in binary mixtures of hard colloidal spheres: Melting of the glass

S. R. Williams and W. van Megen
Department of Applied Physics, Royal Melbourne Institute of Technology, Melbourne, Victoria 3000, Australia
(Received 2 March 2001; published 19 September 2001)

Dynamic light-scattering experiments are performed on binary mixtures of hard-sphere-like colloidal suspensions with a size ratio of 0.6. The optical properties of the particles are such that the relative contrast of the two species is very sensitive to temperature, a feature that is exploited to obtain the three partial coherent intermediate scattering functions. The glass transition is identified by the onset of structural arrest, or arrest of the α process, on the time scale of the experiment. This is observed in a one-component suspension at a packing fraction of 0.575. The intermediate scattering functions measured on the mixtures quantify how, on introduction of the smaller spheres, the α process is released, i.e., how the glass melts. Increasing the fraction of smaller particles causes the α process to speed up but, at a given wave vector, also incurs a change to its amplitude in proportion to the change in the (partial) structure factor.

DOI: 10.1103/PhysRevE.64.041502 PACS number(s): 64.70.Pf, 61.20.Ne, 82.70.Dd

I. INTRODUCTION

Colloidal suspensions of spherical particles, stabilized against coagulation by thin oligomeric layers attached to their surfaces, show a transition from a disordered to an ordered arrangement of particles that mimics the freezing transition predicted for perfect hard spheres [1]. On the strength of this, these suspensions are considered as valuable and, moreover, the only experimental models of the hard-sphere system in which significant structural rearrangements occur in resolvable and accessible time frames [2]. Furthermore, a small spread in particle radii inherent in all laboratory prepared suspensions (typically 5% relative to the mean radius) causes an appreciable delay in nucleation and crystal growth [3], while having little influence on the equilibrium phase behavior [4]. This prolongs the lifetimes of metastable fluid states so that their structure and dynamical properties can be unambiguously identified [5]. Once a certain volume fraction $\phi_g \approx 0.575$ is exceeded, structural rearrangements become effectively arrested [5,6].

Structural relaxation in these pseudo-one-component hard-sphere suspensions has been extensively studied. All aspects of the density-density correlation function, or intermediate scattering function, measured by dynamic light scattering on suspensions in the vicinity of the glass transition are quantitatively consistent with the predictions of the idealized mode-coupling theory [7].

In this paper, we present results of dynamic light-scattering (DLS) measurements made on mixtures of colloidal hard spheres. To resolve the motions of the species, i.e., to construct the three partial intermediate scattering functions, we exploit novel optical properties of the particles to vary their contrast. Rather than altering the relative optical density of the particles, achieved in neutron scattering by changing the isotopic composition of particles or suspending phase [8], variation in optical contrast in this work relies on differences between the amplitudes of light scattered by the particle core and stabilizing shell. This core-shell interplay is so sensitive to temperature that, at least at selected wave vectors, the contrast between the species can be varied by several orders of magnitude by merely altering the temperature of the sample *in situ* [9].

Where a one-component system of hard spheres is defined entirely by the volume fraction, ϕ, specification of a two-component hard-sphere system requires, in addition, the ratio of radii (small to large), $\gamma = R_2/R_1$, and composition, expressed here by the relative volume fraction ϕ_2/ϕ of the smaller particles. The equilibrium phase behavior of such mixtures has been studied extensively by computer simulation and theoretical methods [10,11]. These predict a variety of phase diagrams that encompass, as γ is decreased from unity, solid solutions, separation into solids of the individual species, and formation of compounds, such as AB_2 and AB_{13}. Experiments on mixtures of hard colloidal spheres with, for example, $\gamma \approx 0.6$ find significant agreement with these calculations, including observation of the predicted AB_2 and AB_{13} structures [11,12]. Experiments also indicate that crystallization, if it occurs at all, is exceedingly slow relative to that typically found for one-component suspensions [12]. It appears, therefore, that metastable fluid or glass states in these binary mixtures persist long enough to study their dynamical properties.

The present dynamic light-scattering study of the metastable fluid states of mixtures, with size ratio $\gamma = 0.6$, is confined to the range of volume fractions and compositions where, on the basis of viscosity measurements, we expect the influence of composition to be significant. The viscosity, at low shear rates, of very dense suspensions of spheres decreases dramatically as the size distribution of spheres is broadened while the overall volume fraction (or solids loading) is held fixed [13]. The greater the volume fraction, the greater the reduction in viscosity produced by the inclusion of even a small amount of a second component of smaller spheres. This property, commonly used to enhance the flow of dense suspensions, may be explained, at least in qualitative terms, by the fact that the packing efficiency of a multicomponent randomly assembled arrangement of spheres is greater than that of a one-component assembly [14].

While ''dilution'' of a one-component suspension with

particles of different radius enhances flow and, by implication, structural relaxation, there is also an attendant reduction of variations in the static structure factor. At short and intermediate delay times, in particular, one therefore anticipates a change in the decay rate of a concentration fluctuation, at a given wave vector, in inverse proportion to the change in the static structure factor. The results presented below expose the emergence of these competing processes as well as the manner in which a structurally arrested arrangement of spheres (colloidal glass) is released by inclusion of a second component.

II. SCATTERING THEORY

Here we briefly review the essential aspects of scattering theory of a two-component assembly of spheres. The measured intermediate scattering function (ISF), $F^{(M)}(q,\tau)$, for wave vector q and delay time τ, of a mixture of components $j=1,2$ is given by [2,8]

$$F^{(M)}(q,\tau)=\frac{1}{\overline{b(q)^2}}\left[\begin{array}{c}\phi_1 b_1(q)^2 F_{11}(q,\tau)+2\sqrt{\phi_1\phi_2}b_1(q)b_2(q)F_{12}(q,\tau)\\ +\phi_2 b_2(q)^2 F_{22}(q,\tau)\end{array}\right], \tag{1}$$

where ϕ_j and $b_j(q)$ are the volume fraction and scattering amplitude of species j,

$$\begin{aligned}\overline{b(q)^2}&=\sum\ \phi_j b_j^2(q),\\ F_{ij}(q,\tau)&=\mathrm{Re}\langle\,\delta\rho_i(q,0)\,\delta\rho_j^*(q,\tau)\rangle,\end{aligned} \tag{2}$$

are the partial ISF's, or auto $(i=j)$ and cross $(i\neq j)$ correlation functions of the number density fluctuations

$$\delta\rho_j(q,\tau)=\sum_{k=1}^{N_j}\langle\exp[i\mathbf{q}\cdot\mathbf{r}_k^{(j)}(\tau)]\rangle. \tag{3}$$

Here $\mathbf{r}_k^{(j)}(t)$ and N_j are the position of the kth particle and number of particles of species j, respectively. At $\tau=0$, Eq. (1) reduces to the measured structure factor,

$$S^{(M)}(q)=F^{(M)}(q,0)=\frac{1}{\overline{b(q)^2}}\left[\begin{array}{c}\phi_1 b_1(q)^2 S_{11}(q)+2\sqrt{\phi_1\phi_2}b_1(q)b_2(q)S_{12}(q)\\ +\phi_2 b_2(q)^2 S_{22}(q)\end{array}\right], \tag{4}$$

where $S_{ij}(q)=F_{ij}(q,0)$ are the partial structure factors. In the experimental sections below, we describe the dynamical properties of the system in terms of the normalized ISF's

$$f^{(M)}(q,\tau)=\frac{F^{(M)}(q,\tau)}{S^{(M)}(q)}\quad\text{and}\quad f_{ij}(q,\tau)=\frac{F_{ij}(q,\tau)}{S_{ij}(q)}. \tag{5}$$

This normalization is achieved here by scaling the measured and partial ISF's to unity at $\tau=0$. For a one-component system, $F^{(M)}(q,\tau)=F(q,\tau)$, $S^{(M)}(q)=S(q)$, and $f(q,\tau)=F(q,\tau)/S(q)$. For a two-component system, the three partial ISF's (or partial structure factors) can be calculated from Eq. (1) [or Eq. (4)] once $F^{(M)}(q,\tau)$ [or $S^{(M)}(q)$] has been measured for three independent pairs of scattering amplitudes, $b_1(q)$ and $b_2(q)$.

III. EXPERIMENTAL METHODS

A. Sample preparation

The polymer particles used in this work are similar to the polymethylmethacrylate particles first introduced by Antl, *et al.* [15] and used subsequently in numerous studies of hard-sphere colloids [1,2,6]. Steeply repulsive (''hard-sphere''-like) interactions are produced by solvated layers of poly-12-hydroxystearic acid, approximately 10 nm thick, that are chemically grafted to the particles. The cores of the particles used here are composed of a copolymer of methylmethacrylate (MMA) and trifluoroethylacrylate (TFEA) [16]. Variation of the ratio MMA: TFEA gives a small but, in the present context, significant variation of the refractive index. Furthermore, when the particles are suspended in *cis*-decalin, the suspensions are only weakly turbid at all volume fractions and, therefore, suitable for light-scattering studies. Table I gives the radii, polydispersities, core compositions, and refractive indices of the two species used. Since the difference between the radii of the two species is significantly

TABLE I. Particle properties.

Species	Radius (nm)	Polydispersity	Weight % TFEA	$n_e^{(i)}$
1	200	6%	16	1.491
2	120	9%	24	1.486

larger than their polydispersities, we will, in the ensuing discussion, regard the mixtures as binary.

Suspensions of the larger particles show the crystallization transition expected of hard spheres. Accordingly, as in previous work [1], we determine the effective hard-sphere volume fraction, ϕ_1, of this species by scaling the sample's calculated volume fraction so that the observed freezing volume fraction is equal to the known freezing volume fraction, $\phi_f = 0.494$, of hard spheres [17]. With this reference, we find [1] that the melting volume fraction of the colloidal crystal is 0.535 ± 0.005. Presumably, due to the polydispersity generally encountered in these suspensions, the observed melting value tends to be lower than that (0.545) expected of perfect hard spheres [1]. The calculated volume fraction is based on dry weight analysis, and the difference between it and the effective hard-sphere volume fraction stems mainly from the steric barrier, which is solvated when the particles are suspended in liquid. Probably due to their larger polydispersity, suspensions of the smaller particles do not crystallize. In this case, an estimate of 11 nm for the thickness of the solvated layer was used to convert calculated to effective hard-sphere volume fractions.

Samples were prepared with total volume fractions, $\phi = \phi_1 + \phi_2$, in the range $0.51 \leqslant \phi \leqslant 0.58$ and compositions $\phi_2/\phi = 0$, 0.05, 0.10, and 0.20 in cylindrical glass cells of 8-mm path length. Samples were tumbled for several hours prior to light-scattering measurements in order to shear-melt any crystals and disperse settled particles.

B. Light-scattering methods

Although the suspensions appear only weakly turbid, the contribution of multiply scattered light to the total scattered intensity may be significant particularly at those wave vectors, such as the positions of form-factor minima, where single scattering is weak. Therefore, scattered intensities were measured mainly with an ALV two-color multiple suppression spectrometer operating with the main blue ($\lambda = 488$ nm) and green ($\lambda = 514$ nm) lines of an argon-ion laser [18]. Corrections for multiple scattering and beam attenuation were made by procedures described in Ref. [9].

Particle form factors $b_j(q)^2$ were obtained from measurements on dilute samples of known concentration of individual species at wave vectors in the range $1.5 \leqslant qR_1 \leqslant 4$ and temperatures between 5 and 28 °C, in steps of one degree. Scattered intensities were then measured on mixtures of known (total) volume fraction and composition at three temperatures, chosen to optimize differences of the contrast ratio, $C = [b_1(q)/b_2(q)]^2$, of the components (see Sec. III) for selected values of qR_1. From these data, the partial structure factors $S_{ij}(q)$ were then calculated by Eq. (4).

The above temperature variations do not, as far as we can ascertain from the phase behavior, influence the hard-sphere nature of the interactions nor the particle dynamics, once the delay time is expressed in terms of the characteristic Brownian time (see below).

Comparison of auto and cross time correlation functions of the blue and green scattered intensities revealed no significant multiple scattering for either the one-component or binary suspensions at the wave vectors and temperatures selected. DLS measurements were therefore performed with a conventional (ALV) spectrometer operating with a He-Ne laser ($\lambda = 633$ nm). The digitized scattered light signal was fed into either an ALV-5000 correlator or a homebuilt interleaved sampling correlator [19] (see below).

When the sample volume fraction is less than about 0.56, fluctuations in the scattered intensity decay in less than about 10 s. Thus, for a measurement lasting several thousand seconds, time and ensemble averages of the intensity autocorrelation function (ACF) are equivalent, i.e.,

$$g_E(q,\tau) = g_T(q,\tau), \tag{6}$$

where

$$g_{E,T}(q,\tau) = \frac{\langle I(q,0)I(q,\tau)\rangle_{E,T}}{\langle I(q)\rangle^2_{E,T}}. \tag{7}$$

The brackets $\langle\ \rangle_E$ and $\langle\ \rangle_T$ denote ensemble and time averages, respectively.

When ϕ is increased beyond 0.56, the sample's slowest fluctuation times approach the maximum measurement time (set, somewhat arbitrarily, at $T = 5000$ s). By definition, fluctuation times exceed the measurement time once the glass transition is reached. Thus, at these higher volume fractions, on the time scale of the measurements, $g_E(q,\tau) \neq g_T(q,\tau)$, and ensemble-averaged quantities were determined by the following two steps [20].

(i) First, $M = 3600$ measurements of the (normalized) time-averaged intensity ACF, $g_T^{(j)}(q,\tau)$, and intensity, $\langle I(q)\rangle_T^{(j)}$, were made. The duration of each measurement, j, was $T = 12$ s. A computer-controlled stepper motor subjected the sample to a rotation of a few minutes of arc between each measurement. The process essentially provides values of $g_T^{(j)}(q,\tau)$ and $\langle I(q)\rangle_T^{(j)}$ for M independent spatial Fourier components of the sample's concentration fluctuations. From these the ensemble-averaged intensity ACF, $g_E(q,\tau)$, to a maximum delay time $\tau = 10$ s, was calculated from

$$g_E(q,\tau) = \frac{M\Sigma_{j=1}^{M} g_T^{(j)}(q,\tau)[\langle I(q)\rangle_T^{(j)}]^2}{[\Sigma_{j=1}^{M}\langle I(q)\rangle_T^{(j)}]^2}. \tag{8}$$

(ii) The second step, described in detail in Ref. [20], measures the intensity ACF for longer delay times. The procedure entails continuous rotation of the sample at about 0.3 revolutions per second and sequential triggering of each of 3600 correlators in the computer software with a gating time of 10^{-3} s. This process also provides 3600 independent time-averaged quantities, but now over the time window $1 \leqslant \tau \leqslant 4000$ s. Again, $g_E(q,\tau)$ was estimated from these by Eq. (8).

Although, as discussed in Ref. [20], loss of signal due to repositioning errors and spatial integration, resulting from continuous rotation of the sample, is minimal, $g_E(q,\tau)$ obtained by one of the above methods must be scaled so that it overlaps smoothly with the other in the region, $1 \leqslant \tau \leqslant 10$ s. The resulting ensemble-averaged intensity ACF obtained by the combination of these methods spans the time window

$10^{-6} \leqslant \tau \leqslant 4\times 10^{3}$ s. From this the normalized intermediate scattering function $f^{(M)}(q,\tau)$ was calculated in the usual manner by the Siegert relationship [21],

$$g_E(q,\tau) = 1 + c[f^{(M)}(q,\tau)]^2. \tag{9}$$

The factor c arises from spatial integration over the finite detector area and necessitates normalization of the ISF so that $f^{(M)}(q,0)=1$.

After preparation and tumbling, each sample was allowed to relax to a stationary state. This was achieved by delaying accumulation of final data until the intensity ACF's were independent of commencement time. For the glass states, it was necessary to delay the commencement of measurements by at least ten days before waiting time effects moved out of the experimental window.

IV. SINGLE-PARTICLE FORM FACTORS

In the Rayleigh-Debye limit, the scattering amplitude of a particle having a spherically symmetrical optical density $n_j(r)$, embedded in a medium of optical density n_0, is

$$b_j(q) = \frac{4\pi}{v_j}\int dr[n_j(r)-n_0]r^2\frac{\sin(qr)}{qr}, \tag{10}$$

where v_j is the volume of the particle. In neutron scattering [8], variations in the particles' relative optical density, $|n_j(r)-n_0|$, are usually large in comparison with refractive index variations within the particle, so that Eq. (10) can be approximated by

$$b_j(q) = [\overline{n_j}-n_0]\frac{4\pi}{v_j}\int_0^{R_j} dr\, r^2\frac{\sin(qr)}{qr} = \frac{[\overline{n_j}-n_0]}{v_j}p(qR_j), \tag{11}$$

where

$$p(qR) = 4\pi q^{-3}(\sin qR - qR\cos qR), \tag{12}$$

and R_j and $\overline{n_j}$ are the particle's radius and its mean optical density. However, it appears to be difficult in practice to obtain sufficient variation in the relative contrast, $C=[b_1(q)/b_2(q)]^2$, to avoid significant amplification of experimental errors in the solution of Eq. (1) or Eq. (4), particularly in the vicinity of the minima in $b_j^2(q)$, whose positions, by virtue of Eqs. (11) and (12), are independent of $\overline{n_j}$ and n_0.

In light scattering from concentrated suspensions of near micrometer-sized particles, optical densities of all components must be matched closely to the suspending liquid, i.e., $n_j(r)\approx n_0$, otherwise the suspensions are opaque. This restriction clearly precludes adaptation to light scattering of the contrast variation methods employed in neutron scattering. The requirement that $n_j(r)\approx n_0$, in turn, means that refractive index variations in the particles, $n_j(r)$, are important. These can, for our sterically stabilized polymer particles, simply, yet fairly accurately, be expressed by an optically homogeneous core of radius $R_c^{(j)}$ and a thin shell of radius $R^{(j)}=R_c^{(j)}+\delta$ ($\delta \ll R_c^0$) [9]. The scattering amplitude for this model is

$$b_j(q) = (n_c^{(j)}-n_o)p(qR_c^{(j)}) + (n_s-n_o) \times [p(qR^{(j)})-p(qR_c^{(j)})]. \tag{13}$$

Here $n_c^{(j)}$, n_s, and n_0 are the refractive indices of the particle cores, shells, and suspending liquid. Differences between these must be less than about 1% in order to avoid unacceptable levels of multiple scattering [9]. Hence, small changes in relative values of the refractive indices, produced by altering the sample's temperature, change the scattering amplitudes of the core [first term in Eq. (13)] *vis-à-vis* the shell (second term).

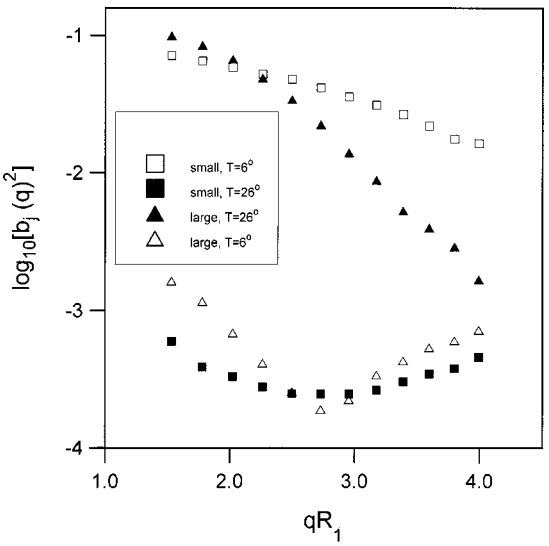

FIG. 1. Single-particle form factors $b_j(q)^2$ (in arbitrary units) shown as functions of the wave vector, qR_1.

The consequences of this are illustrated in Fig. 1, where the single-particle form factors $b_j(q)^2$ of the two species are shown at two temperatures. One sees that at 6 °C, the contrast ratio C is of order 10^{-2} over the range of wave vectors $(1.5 \leqslant qR_i \leqslant 4)$ shown. This ratio is almost inverted when the temperature is increased to 26 °C. Since we measure the ISF's at particular values of q, the form factors are shown in Fig. 2(a) as functions of temperature. This exposes more directly the large variation in the relative contrast of the two species obtained by simply varying the temperature of the sample *in situ*. Although, in principle, any set of three temperatures provides the required three different values of C, the difference in contrast is largest for temperatures $T_1=6$ °C and $T_3=26$ °C, where $C\approx 10^{-2}$ and 10^3, respectively. Thus, at $qR_1=3.0$, $S^{(M)}(q)$ and $F^{(M)}(q,\tau)$ of the mixtures were measured at these temperatures as well as the temperature $T_2=16$ °C chosen somewhat arbitrarily where $C\approx 1$. These results, in combination with the scattering amplitudes at the same temperatures, were then used to solve Eq. (1) or Eq. (4) for the required partial ISF's and structure factors. Typical (matrices of) coefficients of $F_{ij}(q,\tau)$ [Eq. (1)] are listed in Table II for $\phi=0.54$ and two compositions.

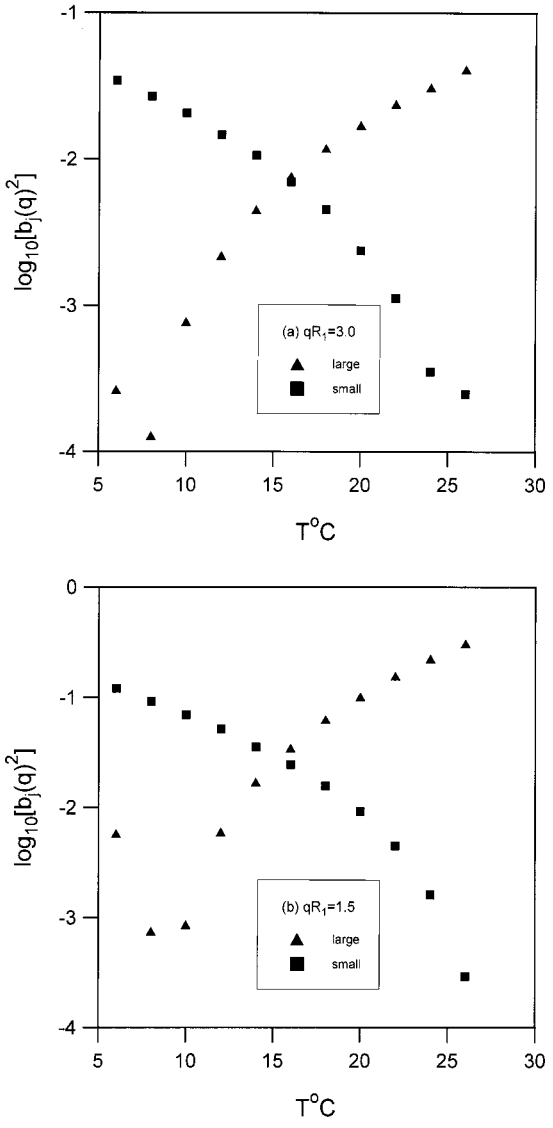

FIG. 2. Single-particle form factors $b_j(q)^2$ vs temperature for (a) $qR_1=3.0$ and (b) $qR_1=1.5$.

The set of temperatures selected for optimum contrast varies with wave vector. At $qR=1.5$, for example [Fig. 2(b)], these are 8, 15, and 26 °C.

Previous analyses [9] of the form factors in terms of the core-shell model [Eq. (13)] reveal that for both species $n_c^{(j)}$ $<n_0$ and $n_s<n_0$, i.e., $b_j(q\rightarrow 0)<0$, when $T\leqslant 6$ °C. From this the sign of the scattering amplitude of each species and, importantly, the sign of the second term on the right-hand side of Eq. (1), are inferred for all T and q.

TABLE II. Coefficients of $F_{ij}(q,\tau)$, in Eq. (1), for different compositions, ϕ_2/ϕ, and temperatures, T, at $qR_1=3.0$ and $\phi=0.58$.

ϕ_2/ϕ	T (°C)	$\phi_1 b_1(q)^2$ $i=j=1$	$2(\phi_1\phi_2)^{1/2}b_1(q)b_2(q)$ $i=1, j=2$	$\phi_2 b_2(q)$ $i=j=2$
0.05	26	6492	149.3	3.43
	14.5	1067	−293.0	80.43
	6	24.67	80.54	262.9
0.20	26	5467	274.0	13.73
	14.5	898.5	−537.7	321.7
	6	20.77	147.8	1051

V. RESULTS AND DISCUSSION

A. Structure factors

To facilitate interpretation of the ISF's, we begin by examining the static structure factors. These also expose any systematic amplification of experimental errors incurred when inverting the above coefficient matrices. The normalized ISF's, $f_{ij}(q,\tau)$ [Eq. (5)], benefit from cancellation of this amplification effect.

Figure 3 shows a comparison between measured and theoretical partial structure factors, $S_{ij}(q)$ for $\phi=0.58$: $S_{11}(q)$ [Fig. 3(a)], $S_{12}(q)$ [Fig. 3(b)], and $S_{22}(q)$ [Fig. 3(c)]. Theoretical results were calculated from the Percus-Yevick approximation [22] with the Verlet-Weiss correction ($\phi\rightarrow\phi-\phi^2/16$). Other work has shown that the results of this approximation compare favorably with experiment [23,24]. We therefore regard the theoretical results as the best estimate of the structure and attribute differences between them and the measured quantities to experimental errors. These differences tend to be largest (>10%) for $S_{12}(q)$ and $S_{22}(q)$, the partial structure factors involving the small particles, when their weighting, ϕ_2/ϕ, is least.

Note that at $qR_1=3$, where the majority of the DLS measurements have been made, $S_{11}(q)$ increases and $S_{12}(q)$ and $S_{22}(q)$ decrease when ϕ_2/ϕ is increased, i.e., the mean-squared amplitude of density fluctuations of the large particles is enhanced while that of the small particles is suppressed. In addition, $S_{12}(q)$ is negative, indicating that density variations of large and small particles, at this wave vector, tend to be out of phase. Figure 3(a) also shows the structure factor $S(q)$ of a one-component fluid at the same total volume fraction, $\phi=0.58$.

The effect of increasing ϕ_2/ϕ on the large particle structure factor is, in some respects, similar to dilution. In this regard, note that increasing ϕ_2/ϕ from zero to 0.2 halves the magnitude of the main peak, a reduction comparable to that expected from simple dilution of a one-component hard-sphere fluid by 20% from an initial volume fraction of 0.58. The difference is that dilution with smaller particles, instead of solvent, shifts the position $q_{\max}$ of the primary maximum to higher q. The other difference is that at $\phi_2/\phi=0.2$ the (large particle) structure factor at $qR_1=1.5$ has increased 10-fold (Table III). Simple dilution would incur an increase by a factor of about 3.

In the shift of the main structure factor peak to higher q and the enhancement, in excess of that obtained by simple dilution, of the mean-squared amplitude of long-wavelength ($q\ll q_{\max}$) fluctuations, one sees the effects of the attractive depletion potential (of mean force) that emerges between the larger particles upon introduction of the smaller particles. The size ratio $\gamma=0.6$ selected here is too large for depletion effects to incur fluid-fluid phase separation [25].

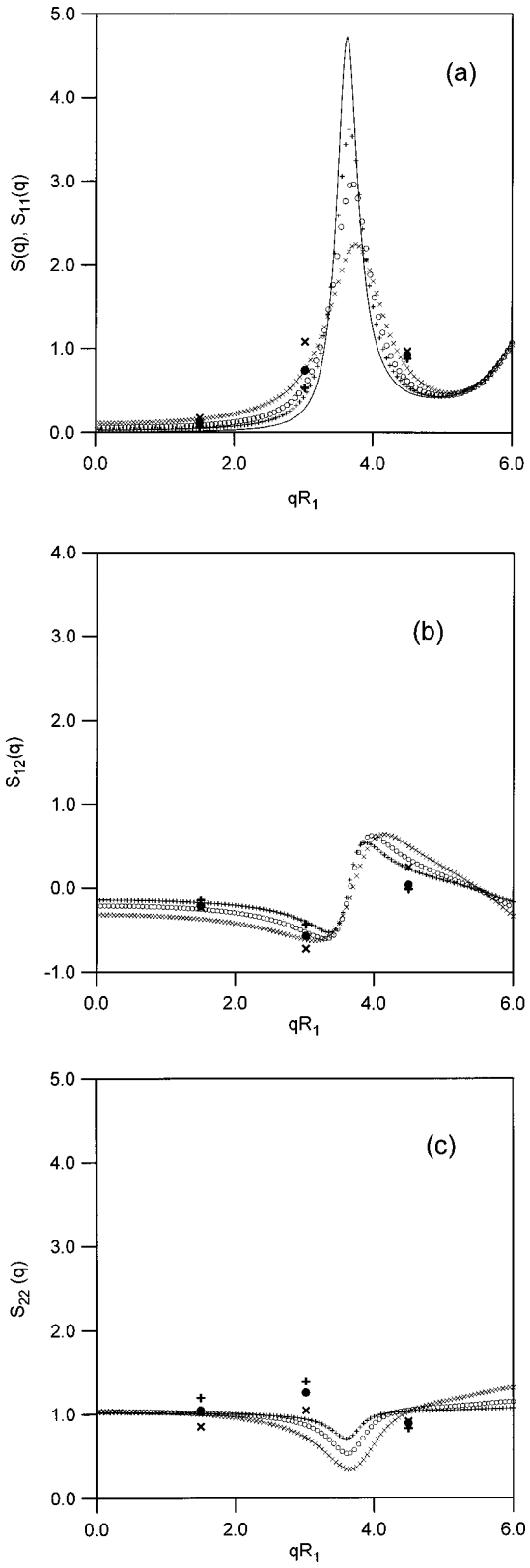

FIG. 3. Partial structure factors (a) $S_{11}(q)$, (b) $S_{12}(q)$, and (c) $S_{22}(q)$ for compositions $\phi_2/\phi=0.05$ (+), $\phi_2/\phi=0.10$ (○), and $\phi_2/\phi=0.20$ (×) and total volume fraction $\phi=0.58$. The light and heavy symbols, respectively, represent Percus-Yevick and experimental results. The solid line in (a) is the structure factor, $S(q)$, of the one-component fluid.

TABLE III. Values of the (large-large particle) structure factor, $S_{11}(q)$, for different values of the wave vector, qR_1, and composition, ϕ_2/ϕ, at $\phi=0.58$. For $\phi_2/\phi=0$, $S_{11}(q)=S(q)$.

ϕ_2/ϕ	$qR_1=1.5$	$qR_1=3.0$	$qR_1=3.6$
0	0.016	0.26	3.13
0.05	0.048	0.42	2.59
0.20	0.16	0.72	1.80

B. Intermediate scattering functions

The results presented here are in the form of the normalized measured and partial intermediate scattering functions, $f^{(M)}(q,\tau)$ and $f_{ij}(q,\tau)$. The dimensionless delay time τ is expressed in units of the characteristic Brownian time, $R_1^2/(6D_0)$ $(=0.021\,\mathrm{s})$, of the large particles, where D_0 is their free diffusion coefficient. Figure 4 shows normalized ISF's $f^{(M)}(q,\tau)$, for $qR_1=3.0$ and $\phi=0.55$, measured at the temperatures and compositions, ϕ_2/ϕ, indicated. The normalized partial ISF's $f_{ij}(q,\tau)$, calculated from them by Eqs. (1) and (4) are also shown. To appreciate the temperature and composition dependence of the difference between $f^{(M)}(q,\tau)$ and $f_{ij}(q,\tau)$, seen in this figure, we refer to Table II, which lists the coefficients of the three (un-normalized) ISF's $F_{ij}(q,\tau)$, appearing in Eq. (1). Normalization of the latter is effected by dividing by their zero time values, $S_{ij}(q)=F_{ij}(q,0)$, which, at $qR_1=3.0$, are all of order unity (see Fig. 3) and will, therefore, have little influence on the relative optical weights listed in Table II.

At $T=26\,^\circ\mathrm{C}$, the coefficient of the $i=j=1$ term (see Table II) exceeds the other two coefficients by more than an order of magnitude. Not surprisingly, $f^{(M)}(q,\tau)$ and $f_{11}(q,\tau)$ are virtually identical, i.e., at $T=26\,^\circ\mathrm{C}$ the scattering properties of the particles are such that the observed fluctuations in the scattered intensity are almost entirely due to the motions of the large particles.

When the temperature is decreased from 26 to 6 °C, the relative contrast, C, of large to small particles is decreased by about five orders of magnitude (see Fig. 2 and Table II). However, even this large reversal of the relative contrast is not sufficient, at least for the small fractions of small particles considered here, to suppress the contribution from the slowly decaying cross-correlation function $f_{12}(q,\tau)$. As a consequence (see Fig. 4), the decay of $f^{(M)}(q,\tau)$, measured at 6 °C, is appreciably slower than $f_{22}(q,\tau)$. Comparing the results in Figs. 4(a) and 4(b), one sees that the difference between $f^{(M)}(q,\tau)$ and $f_{22}(q,\tau)$ at $T=6\,^\circ\mathrm{C}$ decreases as the fraction of smaller particles is increased from 0.05 to 0.2. Nonetheless, this comparison illustrates the difficulty in optically isolating, in a single measurement, the motions or, for that matter, the spatial distribution of the minor component in a mixture.

We now examine in more detail the ISF of the large particles shown in Fig. 5(a) for the wave vector $qR_1=3.0$. One sees, first of all, from the ISF of the one-component suspension of the larger particles that, with increasing volume fraction, there is an increasingly pronounced separation of slow structural rearrangement, or α process, from a faster initial

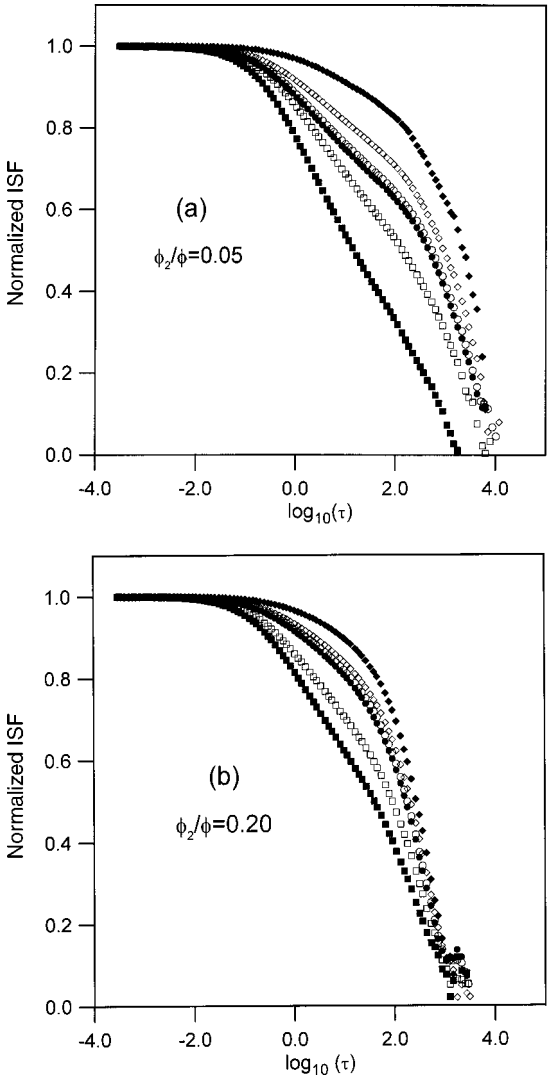

FIG. 4. Normalized intermediate scattering functions vs logarithm of delay time at $\phi=0.54$ for compositions (a) $\phi_2/\phi=0.05$ and (b) $\phi_2/\phi=0.20$. Open symbols indicate measured ISF's, $f^{(M)}(q,\tau)$, at $T=6\,^{\circ}\mathrm{C}$ (squares), 14.5 °C (diamonds), and 26 °C (circles). Closed symbols show the calculated partial ISF's $f_{11}(q,\tau)$ (circles), $f_{12}(q,\tau)$ (diamonds), and $f_{22}(q,\tau)$ (squares).

decay. In fact, for $\phi>0.57$, $f(q,\tau)$ settles to a plateau that remains almost constant to the extremity of the experimental window. This arrest of the α process indicates that the suspension has formed a glass. The height of the plateau, $f(q,\tau\rightarrow\infty)=0.78$ at $\phi=0.58$ for example, represents the fraction of the structure that is arrested [5–7].

These results merely confirm previous observations of a glass transition at $\phi_g=0.575\pm0.005$ in a one-component hard-sphere suspension [5,6]. The ambiguity in ϕ_g arises from the uncertainty in the sample's volume fraction and differences in observation time employed in different experiments.

Turning to the influence of composition, one sees [in Fig. 5(a)] that as ϕ_2/ϕ is increased, the overall decay time of the ISF decreases; this decrease is only marginal for $\phi=0.51$ but is about two decades, when ϕ_2/ϕ is increased from 0 to 0.2,

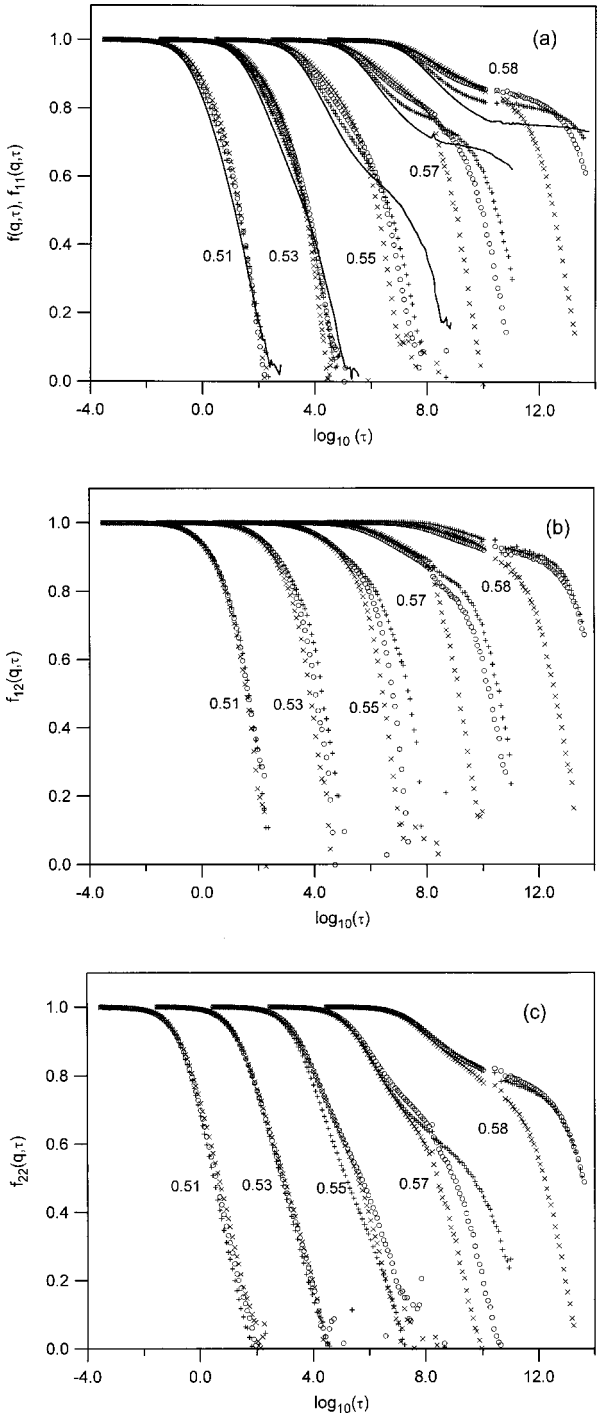

FIG. 5. Intermediate scattering function $f(q,\tau)$ of the one-component suspension (solid lines) and partial intermediate scattering functions, (a) $f_{11}(q,\tau)$, (b) $f_{12}(q,\tau)$, (c) $f_{22}(q,\tau)$, for mixtures at compositions $\phi_2/\phi=0.05$ (+), $\phi_2/\phi=0.10$ (○), and $\phi_2/\phi=0.20$ (×), at $qR_1=3.0$. Successive data sets, at total volume fractions indicated, have been translated along the $\log_{10}(\tau)$ axis by two units.

at $\phi=0.55$. At $\phi=0.58$, introducing the smaller spheres gradually releases the arrested structure until, at $\phi_2/\phi=0.2$, complete structural decay occurs in the experimental window. In qualitative terms at least, the enhancement of structural relaxation observed here is expected since, as seen

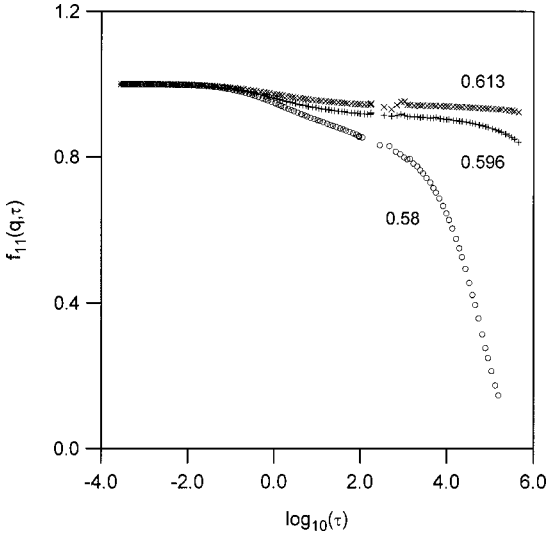

FIG. 6. Partial intermediate scattering functions $f_{11}(q,\tau)$ at $qR_1=3.6$, for the composition $\phi_2/\phi=0.20$ and total volume fractions $\phi=0.58$ (○), $\phi=0.596$ (+), and $\phi=0.613$ (×).

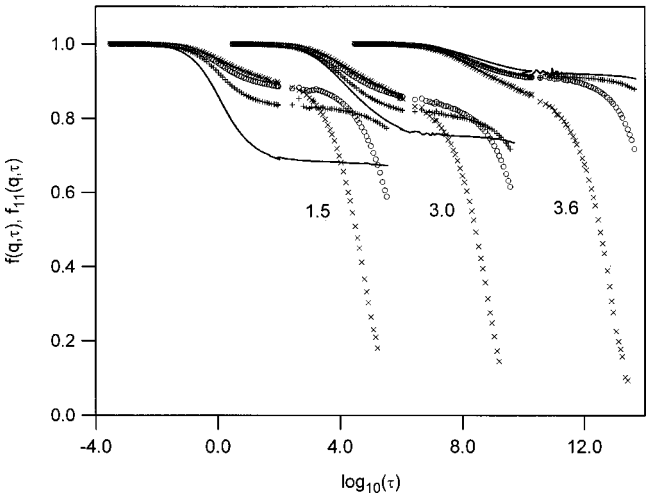

FIG. 7. Intermediate scattering function $f(q,\tau)$ of the one-component suspension (solid lines) and partial intermediate scattering functions $f_{11}(q,\tau)$ for mixtures at compositions $\phi_2/\phi=0.05$ (+), $\phi_2/\phi=0.10$ (○), and $\phi_2/\phi=0.20$ (×), and total volume fraction $\phi=0.58$. Successive data sets, shown for different wave vector, $qR_1=1.5$, 3.0, and 3.6, have been translated along the $\log_{10}(\tau)$ axis by four units.

in Fig. 3, introduction of the second component effectively dilutes the suspension. Figure 6 shows $f_{11}(q,\tau)$ at several volume fractions $\phi \geqslant 0.58$ for the composition $\phi_2/\phi=0.2$. Thus, to obtain structural arrest in this binary mixture, its volume fraction needs to be raised to approximately 0.60.

The enhancement of structural relaxation seen in $f_{11}(q,\tau)$ [Fig. 5(a)], as ϕ_2/ϕ is increased, is also evident in the other two partial ISF's $f_{12}(q,\tau)$ and $f_{22}(q,\tau)$, shown in Figs. 5(b) and 5(c). For reasons already mentioned, there is more noise in the latter quantities, particularly at the higher volume fractions. With due allowance for this, one generally sees that, as ϕ_2/ϕ is increased, $f_{12}(q,\tau)$ and $f_{22}(q,\tau)$ decrease at all delay times. However, $f_{11}(q,\tau)$ increases at short and intermediate times.

To aid our explanation of the decay of the partial ISF's observed at short and intermediate times, we recall known connections between the structure factor and the decay of the ISF for a one-component system. First, the initial decay of a concentration fluctuation is purely diffusive and, hydrodynamic interactions notwithstanding, is characterized by the diffusivity, $D(q)$, which is proportional to $S^{-1}(q)$ [2]. Secondly, the amplitude of the α process has a wave-vector dependence that varies in harmony with $S(q)$ [7]. The latter feature has been predicted by mode-coupling theory [7] and verified by experiment [6] and computer simulation [26]. We therefore expect that the larger $S(q)$ is, the slower will be the initial diffusive decay of the ISF and the larger the amplitude of the α process.

From the partial structure factors (Fig. 3), we have already noted that, at $qR_1=3.0$, $S_{11}(q)$ increases while $S_{12}(q)$ and $S_{22}(q)$ decrease with increasing ϕ_2/ϕ. Now we see that this influence of composition on $S_{ij}(q)$ is reflected in the decay of the corresponding partial ISF's at short and intermediate times. This is most evident in $f_{11}(q,\tau)$ at the highest volume fractions [Fig. 5(a)]. One sees that the initial decay rate decreases and the amplitude of the α process, inferred from the height of the plateau or shoulder, increases, but sets in earlier, with increasing ϕ_2/ϕ. While the influence of composition on the initial and intermediate decay of the other two partial ISF's is compatible with that seen in their corresponding partial structure factors, the connection is less convincing. One reason is that, at this wave vector, $S_{11}(q)$ is more sensitive to changes in composition than either $S_{12}(q)$ or $S_{22}(q)$. Also, as already mentioned, there is more experimental noise in $f_{12}(q,\tau)$ and $f_{22}(q,\tau)$.

To explore further the connection between the structure factor and the ISF, Fig. 7 shows plots $f_{11}(q,\tau)$ at $\phi=0.58$

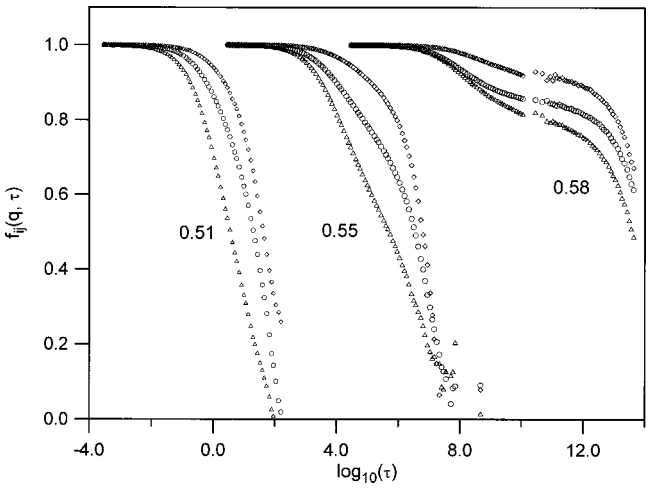

FIG. 8. Partial intermediate scattering functions $f_{11}(q,\tau)$ (circles), $f_{12}(q,\tau)$ (diamonds), and $f_{22}(q,\tau)$ (triangles) of mixtures at composition $\phi_2/\phi=0.10$. Successive data sets, shown for total volume fractions $\phi=0.51$, 0.55, and 0.58, have been translated along the $\log_{10}(\tau)$ axis by four units.

for several wave vectors. Examination of this figure in conjunction with Table III (and Fig. 3) indicates that the change to the amplitude of the α process, incurred when ϕ_2/ϕ is increased, is in harmony with the change in $S_{11}(q)$ relative to $S(q)$. The larger increase in the amplitude of the α process for $qR_1=1.5$, compared with that seen for $qR_1=3.0$, reflects the larger increase in $S_{11}(q)$. Close to the position $qR_1=3.7$ of the maximum in the structure factor, $S_{11}(q)$ decreases relative to $S(q)$ on inclusion of the second component. In this case, we see that the amplitude of the α process decreases. As shown above, dilution of the suspension with the second component increases the rate of structural relaxation and gradually obscures the separation in time of the α process from the early part of the decay.

Finally, Fig. 8 shows all three partial ISF's for the composition $\phi_2/\phi=0.2$. At short and intermediate times, the faster decay of $f_{22}(q,\tau)$, in comparison with that of $f_{11}(q,\tau)$, reflects the higher mobility of the smaller particles. Relaxation of $f_{12}(q,\tau)$ requires exchange of species and is, at short and intermediate times, the slowest. This comparatively slow decay of $f_{12}(q,\tau)$ may be one reason for the slow crystallization observed in hard-sphere mixtures where the formation of the solid requires segregation of the components.

VI. CONCLUSIONS

Partial structure factors and partial intermediate scattering functions have been measured by light scattering for binary colloidal mixtures of particles with hard-sphere interactions. This study has examined the influence of composition on the ISF's and their connection to the structure factors, particularly at volume fractions in the vicinity of the glass transition. From these experiments, we conclude the following. First, inclusion of a second component while keeping the total volume fraction fixed enhances the α process. In a colloidal glass, this process is arrested but may be released and the glass ''melted'' by increasing the fraction of the second component. Second, the initial (diffusive) decay rate of the partial ISF's with composition varies inversely, as expected from cumulant expansions, with the corresponding partial structure factors. Third, amplitudes of the α processes in the partial ISF's also reflect the composition and wave-vector dependence of the partial structure factors.

ACKNOWLEDGMENTS

We are grateful to G. Bryant and W. Götze for comments on the manuscript and to P. Francis for technical assistance. This work was supported by the Australian Research Council.

[1] P. N. Pusey and W. van Megen, Nature (London) **320**, 340 (1986); S. E. Paulin and B. J. Ackerson, Phys. Rev. Lett. **64**, 2663 (1990); S. M. Underwood, J. R. Taylor, and W. van Megen, Langmuir **10**, 3550 (1994).

[2] P. N. Pusey, in *Liquids, Freezing and the Glass Transition*, edited by J. P. Hansen, D. Levesque, and J. Zinn-Justin (North-Holland, Amsterdam, 1991), p. 763; P. Bartlett and W. van Megen, in *Granular Matter*, edited by A. Mehta (Springer-Verlag, New York, 1994), p. 195.

[3] I. Moriguchi, K. Kawasaki, and T. Kawakatsu, J. Phys. II **5**, 143 (1995); S. I. Henderson and W. van Megen, Phys. Rev. Lett. **80**, 877 (1998).

[4] P. G. Bolhuis and D. A. Kofke, Phys. Rev. E **54**, 634 (1996); D. A. Kofke and P. G. Bolhuis, *ibid.* **59**, 618 (1999).

[5] W. van Megen and P. N. Pusey, Phys. Rev. A **43**, 5429 (1991).

[6] W. van Megen and S. M. Underwood, Phys. Rev. E **47**, 248 (1993); **49**, 4206 (1994).

[7] W. Götze, J. Phys.: Condens. Matter **11**, A1 (1999).

[8] P. Bartlett and R. H. Ottewill, J. Chem. Phys. **96**, 3306 (1992); H. J. M. Hanley, G. C. Straty, and P. Lindner, Langmuir **10**, 72 (1994).

[9] G. Bryant, T. Mortensen, S. Henderson, S. Williams, and W. van Megen, J. Colloid Interface Sci. **216**, 401 (1999).

[10] A. R. Denton and N. W. Ashcroft, Phys. Rev. A **42**, 7312 (1990); W. G. T. Kranendonk and D. Frenkel, Mol. Phys. **72**, 679 (1991).

[11] M. D. Eldridge, P. A. Madden, P. N. Pusey, and P. Bartlett, Mol. Phys. **84**, 395 (1995).

[12] P. Bartlett, R. H. Ottewill, and P. N. Pusey, J. Chem. Phys. **93**, 1299 (1990); Phys. Rev. Lett. **68**, 3801 (1992).

[13] R. L. Hoffman, J. Rheol. **36**, 947 (1992).

[14] A. P. Shapiro and F. Probstein, Phys. Rev. Lett. **68**, 1422 (1992).

[15] L. Antl, J. W. Goodwin, R. D. Hill, R. H. Ottewill, S. M. Owens, S. Papworth, and J. Waters, Colloids Surface **17**, 67 (1986).

[16] S. M. Underwood and W. van Megen, Colloid Polym. Sci. **274**, 1072 (1996).

[17] W. G. Hoover and F. H. Ree, J. Chem. Phys. **49**, 3609 (1968).

[18] P. N. Segrè, W. van Megen, P. N. Pusey, K. Schätzel, and W. Peters, J. Mod. Opt. **42**, 1929 (1995).

[19] J. Müller and T. Palberg, Prog. Colloid Polym. Sci. **100**, 121 (1996).

[20] W. van Megen, T. C. Mortensen, S. R. Williams, and J. Müller, Phys. Rev. E **58**, 6073 (1998).

[21] P. N. Pusey, in *Photon Correlation Spectroscopy and Velocimetry*, edited by H. Z. Cummins and E. R. Pike (Plenum, New York, 1977).

[22] P. van Beurten and A. Vrij, J. Chem. Phys. **74**, 2744 (1981).

[23] C. G. de Kruif, W. J. Briels, R. P. May, and A. Vrij, Langmuir **4**, 668 (1988).

[24] S. R. Williams (unpublished).

[25] T. Biben and J-P. Hansen, Phys. Rev. Lett. **66**, 2215 (1991).

[26] T. Gleim, W. Kob, and K. Binder, Phys. Rev. Lett. **81**, 4404 (1998).